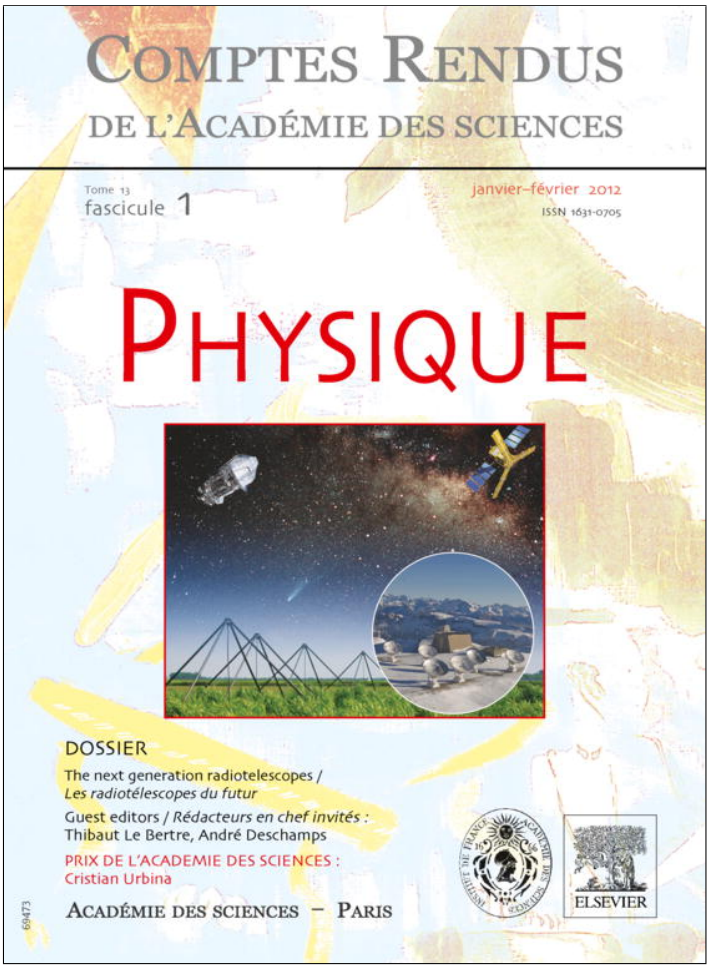

C. R. Physique 13 (2012) 62–70

Contents lists available at SciVerse ScienceDirect

Comptes Rendus Physique

www.sciencedirect.com

The next generation radiotelescopes / Les radiotélescopes du futur

Kinetic inductance detectors for millimeter and submillimeter astronomy

Détecteurs à inductance cinétique pour l'astronomie millimétrique et sub-millimétrique

Nicolas Boudou [a], Alain Benoit [a], Olivier Bourrion [c], Martino Calvo [a], François-Xavier Désert [b], Juan Macias-Perez [c], Alessandro Monfardini [a,*], Markus Roesch [d]

[a] *Institut Néel, CNRS and université de Grenoble, BP 166, 38042 Grenoble cedex 9, France*
[b] *Laboratoire d'astrophysique, observatoire de Grenoble (LAOG), BP 53, 38041 Grenoble cedex 9, France*
[c] *Laboratoire de physique subatomique et de cosmologie (LPSC), 53, rue des Martyrs, 38026 Grenoble, France*
[d] *Institut de radioastronomie millimétrique (IRAM), 300, rue de la piscine, 38406 Saint Martin d'Hères, France*

ARTICLE INFO

Article history:
Available online 11 December 2011

Keywords:
Millimeter astronomy
Superconducting detectors
Kinetic inductance
Multiplexed electronics

Mots-clés :
Astronomie millimétrique
Détecteurs supraconducteurs
Inductance cinétique
Électronique multiplexée

ABSTRACT

We present recent developments in Kinetic Inductance Detectors (KID) for large arrays of detectors. The main application is ground-based millimeter wave astronomy. We focus in particular, as a case study, on our own experiment: NIKA (Néel IRAM KID Arrays). NIKA is today the best in-the-field experiment using KID-based instruments, and consists of a dual-band imaging system designed for the IRAM 30 meter telescope at Pico Veleta. We describe in this article, after a general context introduction, the KID working principle and the readout electronics, crucial to take advantage of the intrinsic KID multiplexability. We conclude with a small subset of the astronomical sources observed simultaneously at 2 mm and 1.4 mm by NIKA during the last run, held in October 2010.

RÉSUMÉ

Nous décrivons les récents développements concernant les grandes matrices de détecteurs à inductance cinétique (KID) dont l'application principale est l'astronomie millimétrique au sol. Nous détaillons en particulier notre propre caméra : NIKA (Néel IRAM KID Arrays) qui est aujourd'hui l'instrument le plus abouti mettant en œuvre des KIDs. NIKA est une caméra bi-bande conçue pour le radiotélescope de 30 mètres de l'IRAM à Pico Veleta. Après avoir décrit le contexte instrumental dans lequel ils s'inscrivent, nous expliquerons le principe de fonctionnement des KIDs et de leur électronique de lecture, cruciale pour pouvoir tirer parti de leur potentiel de muliplexage. Pour finir, nous présentons quelques exemples d'observations effectuées par NIKA dans les bandes de 2 mm et 1,4 mm au cours de la dernière campagne d'observation en octobre 2010.

* Corresponding author.
E-mail addresses: nicolas.boudou@grenoble.cnrs.fr (N. Boudou), alain.benoit@grenoble.cnrs.fr (A. Benoit), olivier.bourrion@lpsc.in2p3.fr (O. Bourrion), martino.calvo@grenoble.cnrs.fr (M. Calvo), francois-xavier.desert@obs.ujf-grenoble.fr (F.-X. Désert), juan.macias-perez@lpsc.in2p3.fr (J. Macias-Perez), alessandro.monfardini@grenoble.cnrs.fr (A. Monfardini), roesch@iram.fr (M. Roesch).

1631-0705/$ – see front matter
doi:10.1016/j.crhy.2011.10.008

1. Introduction

The last decades saw an increasing importance of millimeter and submillimeter observations for cosmology and astrophysics. The discovery of the Cosmic Microwave Background (CMB) at 1.9 mm wavelength and its temperature anisotropies provided an unprecedented understanding of the early universe and of the formation of galaxies [1,2]. More recently, studies of the CMB revealed the Sunyaev–Zel'dovich effect which one can use to map the distribution of hot gases in clusters of galaxies [3]. Millimeter wavelengths are also vital for observations of dust emission in galaxies and molecular clouds known to be central to star formation.

Ultrasensitive cryogenic detectors are necessary to access the low energy millimetric spectrum. Until now, dominating technologies use low temperature bolometers. Constant improvements brought these detectors to full maturity. Since their performance has already reached the background noise level, a large array of detectors is the only remaining solution for greater sensitivity and higher mapping speed. However, the limited cryogenic cooling power, ranging from nW to mW, limits the amount of read-out wires entering the cryostat. Massive efforts in the development of multiplexing techniques have produced state-of-the-art instruments (e.g. SCUBA2 [4], LABOCA [5]) that typically employ several thousands of pixels. In spite of it all, resulting complexity of read-out electronic, as well as cryogenic logistic severely, limit higher multiplexing ratios for that type of detector.

In this context emerged a new technology based on an innovative detector intrinsically adapted to frequency-domain multiplexing: the Kinetic Inductance Detector (KID). Firstly presented in 2003 [6], this device rapidly became a promising alternative to bolometers benefiting from parallel research in quantum computing [7] and fundamental physics. A KID consists of an energy sensitive superconducting resonator typically working between 1 GHz and 10 GHz. Its high quality factor (up to a million) virtually allows multiplexing of several thousands of detectors on a single transmission line. Throughout the last years a new generation of instruments making use of KID arrays appeared: MUSIC [8] (MUltiwavelength Sub/millimeter kinetic Inductance Camera) for the Caltech Submillimeter Observatory (CSO), the KID camera for the Atacama Pathfinder EXperiment (APEX), and the Néel IRAM KID Arrays (NIKA), a project carried out by our group [9,10]. NIKA has already been tested twice on the Institute for Millimetric Radio Astronomy (IRAM) 30 meter telescope at Pico Veleta and gave promising results with the aim of a permanent stay.

In this article we expose KID-based camera nascent technology emphasizing on the detector measurement operation. We will then present results from the latest NIKA run held in October 2010.

2. Kinetic inductance detectors

In the superconducting regime, current is carried by Cooper pairs with a binding energy $2\Delta g \approx 3.528 k_B T_c$ with Δg the superconducting energy gap, k_B the Boltzmann constant and T_c the superconducting transition temperature. As these boson-like carriers do not transfer energy to the crystal lattice, energy may be stored in the form of kinetic energy. In case of an alternating current, however, an electrical reactance is observed which originates from this stored energy. It is very common to associate to this effect a kinetic inductance. An incoming photon with sufficient energy $h\nu > 2\Delta g$ may break Cooper pairs into quasiparticles. These non-equilibrium particles recombine into Cooper pairs after $\tau_{qp} \approx 10^{-6}$–$10^{-3}$ s. The increase of the quasiparticle population affects the surface impedance Zs of the material. Using this change in Zs to detect radiation absorption is the underlying concept in kinetic inductance detectors. KIDs are actually microwave resonant circuits made of superconducting material. The KID specific geometry (low volume, thin film planar structure) together with a high quality factor Q ensure a large response to changes in quasiparticles density. Practically, measurements consist in monitoring the transmitted phase and amplitude of a fixed tone set on the resonant frequency. Changes in Zs produce detectable resonance frequency shifts of the device. The measurement operation is displayed in Fig. 1.

When designing a KID, the resonance frequency is tuned by setting the length of the resonant section. This, together with a high Q, allows a high rate KID multiplexing, up to a thousand on a single transmission line. The design of the coupling area between the resonator and the feedline is also of importance as it affects the external quality factor Qe. Moving the KID away from the feedline will increase Qe, but will also shrink the resonance dip. The use of electromagnetic simulation tools is unavoidable to find a good trade-off. Performance of KID devices depends on multiple parameters: as stated above the sensitivity is related to geometrical aspects such as device volume and film thickness but not only. As for other pairs-breaking detectors, the KID sensitivity scales with quasiparticles lifetime τ_{qp} (at least for a low energy photon stream) which is material related, but also depends on the quality of the deposition process. Material choice affects the sensitivity for another reason: It determines the value of kinetic inductance in the resonant circuit. Photon frequency detection threshold is governed by the energy gap: $\nu_{\min} = 2\Delta g/h = 3.528 k_B T_c/h$. So far, millimeter-wave applications mostly use aluminum ($\nu_{\min} = 103$ GHz for thin films) but development of TiN films ($\nu_{\min} = 77$ to 403 GHz) with a larger kinetic inductance should provide improvements in sensitivity [11]. The KIDs' noise fundamental limitation comes from the quasiparticles generation and recombination which is material dependent. However, current intrinsic device noise is limited by dielectric surface defects [12]. As for now two main KID designs have been proposed. The first one known as distributed KID consists of a standard quarter-wave CoPlanar Waveguide (CPW) whose short-ended extremity is coupled to an antenna. Micro-lenses are usually employed to focus the radiation on the antenna. Associated with microwave filters, this approach allows frequency selective applications. Our group opted for the second configuration referred to as Lumped Element KID (LEKID [13]), in opposition to the previous one. LEKID comprises a distinct meander section and a interdigital capacitor. The

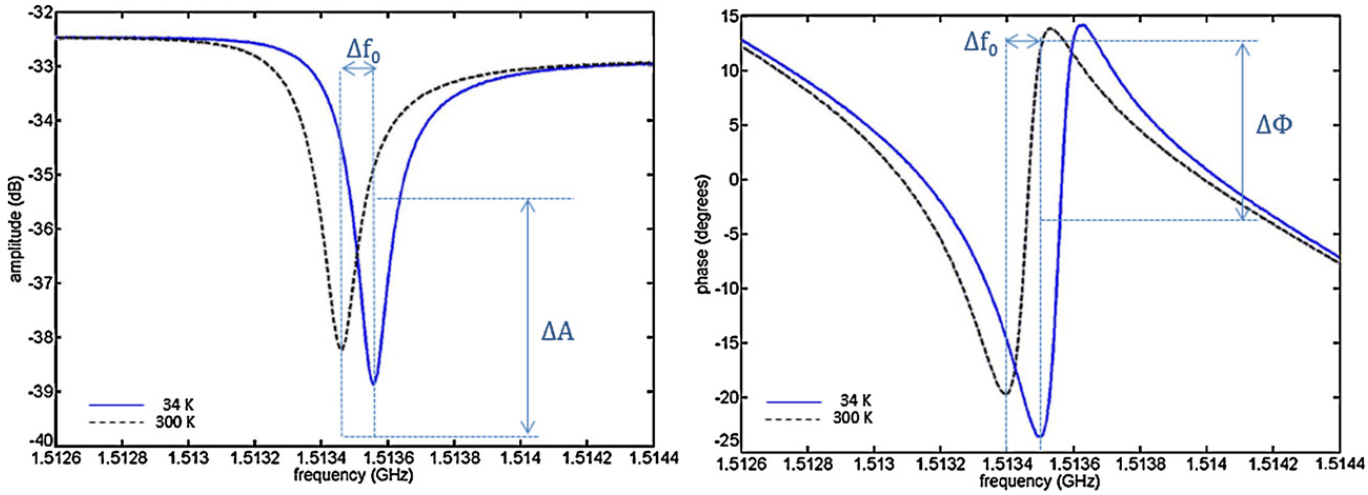

Fig. 1. KID measurement operation: amplitude and phase responses of KID. Solid lines are measured resonance under dark conditions while dashed lines are under illumination.

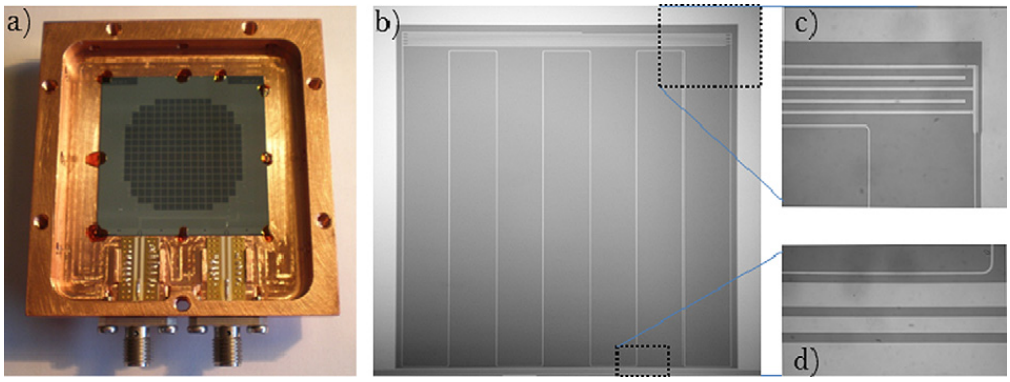

Fig. 2. Mounted arrays and pixel micrographs. (a) 144-pixel LEKID array. (b) LEKID pixel micrograph, dark regions are silicon, bright areas are aluminum. (c) Enlarged view of the interdigital capacitor and (d) the coupling area.

meander exhibits no current variation along its length and also acts as an absorber on itself. By tuning the width and the number of meandered lines one can impedance match the meander area to the free space. On its simplest version (see Fig. 2) LEKIDs are mostly sensitive to a single polarization but there is no particular issue in building a meander sensitive to both polarizations [14]. Finally, optical coupling is achieved using a reflective back-short tuned to the band of interest. This device employing only one layer of metal, its fabrication stays very simple; thin aluminum film is evaporated on a 375 µm thick high resistivity ($\rho > 1000\ \Omega\,\mathrm{cm}$) silicon wafer. Removing the substrate native oxide is achieved by argon milling prior to deposition. The device is subsequently patterned using optical lithography and wet etching.

Using KIDs in large arrays also brings specific problems. The most notable one is the displacement and overlapping of resonances because of cross-talk between different resonators. Practically, this means that a certain number of resonators (or pixels in case of an imaging array) are lost. As this effect becomes stronger with larger arrays, it becomes an obstacle for future giant multiplexing strategies and has therefore drawn the attention of the KID community, but so far no efficient strategy has been proposed to address that issue. To a lesser extent, due to their increasing size, KID arrays also show a high susceptibility to defects. This requires additional care during the fabrication process.

3. Multiplexing readout electronics

The strongest point in using KID detectors compared to more classical bolometers is the ability to multiplex many channels on the same read-out electronics. It is useful here to describe in more detail the actual way of running multiple resonators on the same line. Our FPGA-based prototype digital multiplexing electronics requires only two (IN/OUT) coaxial cables for reading out a 128-pixel array, with resonances spread over 125 MHz of bandwidth. An excitation comb of frequencies is generated and fed through the detector by a fast (250 MSPS) DAC (Digital to Analog Converter). The relative positions of the tones in the comb correspond exactly to the resonators on the array. The direct frequency synthesis and the data acquisition rely heavily on a large FPGA using parallelized and pipelined processing. As the KID resonant frequencies can easily be controlled during manufacturing, and the quality factor is huge, it is possible to couple a large number of them to a single transmission line. The multiplexing factor N is at present limited, mainly, by the available bandwidth. It will be possible, however, in the future, to apply the same concept and deal with thousands of pixels. In any case, even if

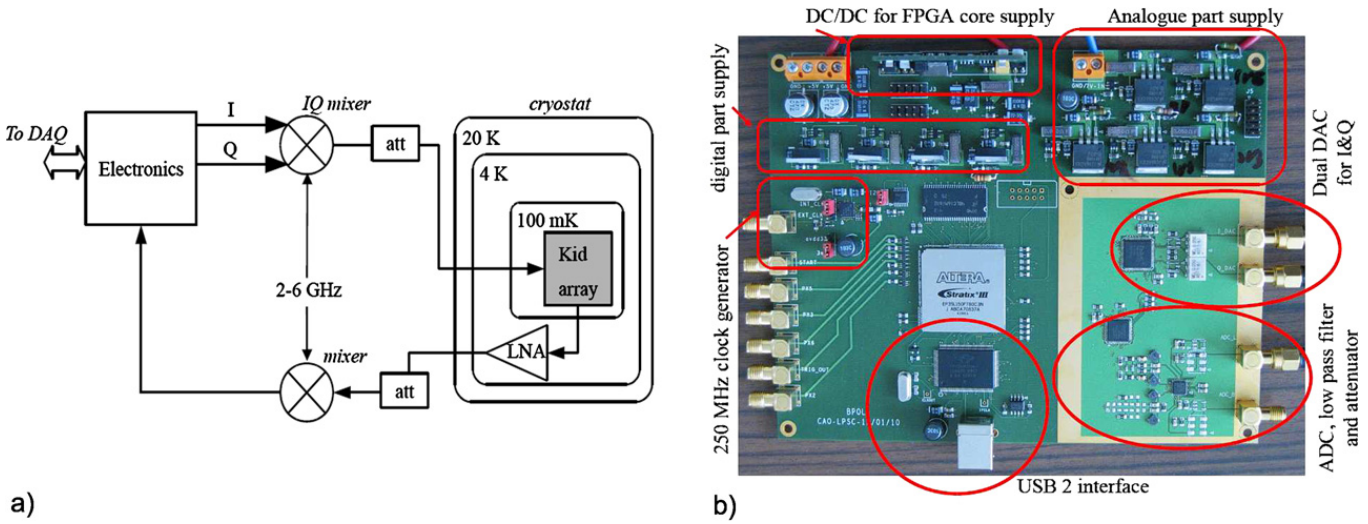

Fig. 3. (a) KID readout electronics scheme. (b) Picture of the prototype FPGA board [17] realized for NIKA and able to achieve a multiplexing factor $N = 128$.

$N = 128$, it is still possible to feed more than two cables into the cryostat. For example, we foresee using up to 12 lines for the next generation resident IRAM continuous instrument (see Section 6). The comb generated by the FPGA is up-converted by a single IQ mixer up to the multi-GHz KID band. After the resonators, the comb itself is down-converted again by a second, identical IQ mixer referenced with a copy of the LO (Local Oscillator). At the output of the transmission line coupled with the KID, the resultant signal must be acquired and analyzed in order to determine the time dependent phase and amplitude variation of each sinusoid. Two different solutions can be implemented in order to perform these operations. The first obvious one is based on the Fast Fourier Transform (FFT) analysis. In that case, the comb of frequencies, composed of summed sinusoids, is calculated off-line, stored in a circular buffer and used as the KID array excitation signal. Then, the signal having interacted with the resonators is acquired and analyzed either off-board by dedicated computers or on-board by means of DSPs or FPGA [15]. In the first implementation a small size FPGA coupled to memories (stimulation and acquisition buffers) is sufficient and allows one to easily cover a large bandwidth as the hardware processing power is reduced to a minimum. In the second case, a larger FPGA coupled to buffers holding stimulus and featuring a FPGA adapted FFT algorithm (channelizer) is used in order to maintain an acceptable read-out rate (up to a 100 Hz with 131×10^3 frequency bins) [16].

The second method, allowing larger data frame rates and thus chosen for our application, is also known as channelized Direct Down Conversion (DDC). In this case the frequency comb is built in real time by summing as many tones as necessary. Then, after propagation of the excitation signal through the MKID array, the resulting signal is processed for each tone by a dedicated DDC. The incoming signal, containing all the frequencies of the comb, is at first split in two branches and multiplied by the sine and cosine waves of the tone of interest and finally low pass filtered in order to keep only the lower side band, i.e. the baseband, of the signal. The In (I) phase and Quadrature (Q) component of the tone are thus obtained. In the base configuration, adopted for example in the 2010 telescope run whose results are presented in Section 5, the data stream to the DAQ (Data AcQuisition) consists simply in a series of $(\mathrm{I}, \mathrm{Q})_i$ pairs $(i = 1, \ldots, N)$, properly averaged for a final frame rate of 20–25 Hz. By combining the (I, Q) values for each pixel with a calibration frequency sweep performed before each on-the-fly scan, we could extract the pixel frequency shifts, proportional at the first order to the incoming power. The final signal for a KID-based pixel is thus expressed in Hz, and the noise is measured in $\mathrm{Hz}/\mathrm{Hz}^{0.5}$. For example, when Mars (roughly 40 Jy at 2 mm during the 2010 NIKA run described in more detail in the astronomical results section) transits on one NIKA pixel, the resonating frequency shifts by about 4 kHz. The frequency noise at the representative frequency of 1 Hz is 2 $\mathrm{Hz}/\mathrm{Hz}^{0.5}$. As a result, Mars is detected with signal-to-noise ratio of 2000 $\mathrm{Hz}^{0.5}$. In order to improve the photometric calibration, the reference frequency of the up/down converter can be modulated at a frequency of about 500 Hz. In this way, we can measure in real time, for each frame and for each pixel, besides the (I, Q) point coordinates, a $(\mathrm{dI}, \mathrm{dQ})$ vector proportional to the very pixel sensitivity. This procedure has been implemented in 2011, and will be tested during the next run on the telescope, planned for October 2011.

4. The Néel IRAM KID arrays

NIKA instrument is intended to equip the Pico Veleta IRAM 30 meter telescope. In order to ease logistics in the telescope environment, NIKA cryogenics is helium-free. A pulse-tube refrigerator is used for pre-cooling, then a dilution cryostat enables a base temperature of 60 mK. During observation runs, the whole instrument stays still thanks to a rotating mirror. NIKA camera projects the telescope focal plane on the detectors arrays by the use of two flat mirrors (M6 and M7), one bi-polynomial mirror (M8) and three High-Density PolyEthylene (HDPE) lenses. This results in a focal plane scale of 5 arcseconds/mm on the detector plane. Lenses are placed on the 300 K and 4 K screens, and just in front of the detector

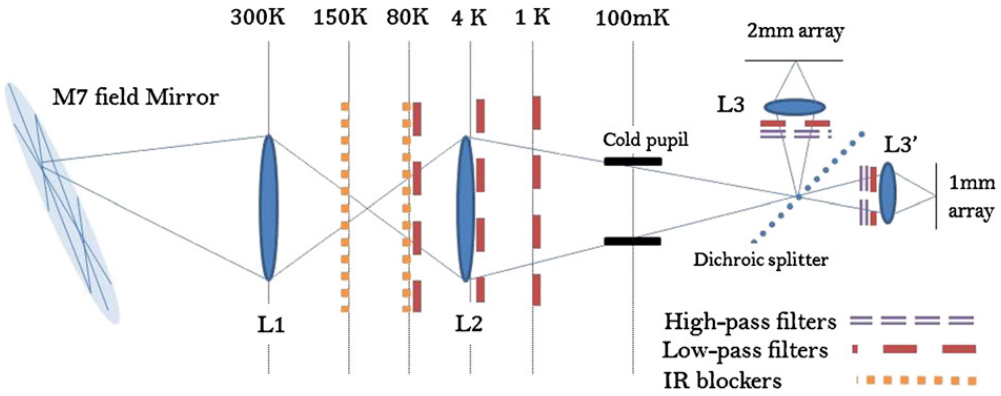

Fig. 4. NIKA optical design. The rays enter the cryostat through the window, coincident with lens L1. The dichroic splitter divides the beam and redirects the radiation to two arrays, the first optimized for 150 GHz, the second for 220 GHz. Band defining filters are mounted directly in front of the flat face of each L3 lens.

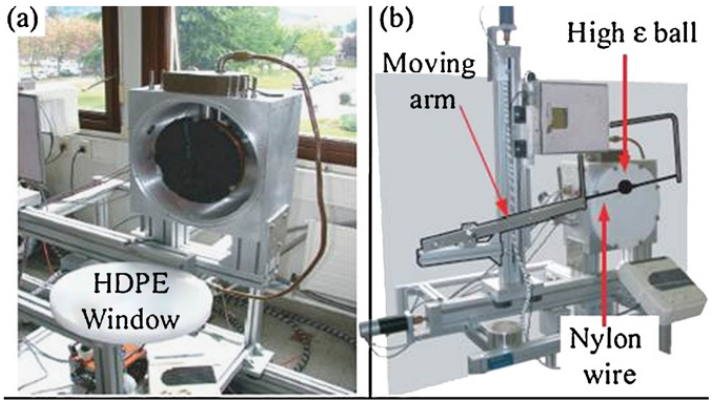

Fig. 5. Sky simulator. (a) The cold disk simulating the sky background is shown; its diameter is 24 cm. During operation a 4 cm thick HDPE window provides a suitable transparency in millimeter wavelengths. (b) Fully assembled system. The translation arm, nylon wire and high emissivity ball are outlined for visibility. The ball moves at a controlled rate faking a real source on the sky.

samples. HDPE lenses are highly transparent in the millimeter region so that their contribution to the optical loading is not significant in comparison to the sky background. These lenses are telecentric; every detector sees the source with the same aperture and with the chief ray perpendicular to the KID surface, this in order to reduce systematic errors coming from differences in pixels lobes. In order to reject unwanted radiation, the cryostat is equipped with a series of filters: 150 K and 80 K screens are fit with IF blocking filters while low-pass cross mesh filters reflect radiation with $\nu > 300$ GHz on the 80 K, 4 K and 1 K screens. Additionally, a Stycast® based black-coated baffle in the 4 K area together with a cold pupil at 70 mK prevent stray light effects. Within the 100 mK area, the beam is divided in two by the use of a 45° oriented dichroic splitter made of a superposition of metallic cross mesh foils. Dichroic transmission spreads from 190 GHz to 270 GHz while lower frequencies are reflected back. Filtering is completed by low-pass and high-pass filters positioned in front of the 2 mm and 1 mm array respectively. The overall NIKA optical scheme is presented in Fig. 4. The spectral response of NIKA was characterized using a Martin-Puplett interferometer [10]. The LEKID device, mounted on the 2 mm channel, exhibit a bandwidth in good agreement with the atmospheric transparency window (125–170 GHz). Camera equipment also comprises a lead shield positioned on the 4 K screen that prevents magnetic field fluctuations. Currently, detector arrays are made of 144 aluminum pixels, covering a surface of 19.2 by 19.2 and 27 by 27 mm^2 for the 1 mm and 2 mm matrix respectively. The resulting useful field of view is 1.6 by 1.6 arcminutes for the 2 mm array and 1 by 1 arcminute for the 1 mm array. In order to replicate real observing conditions, we have built a testing tool to complement Martin-Puplett interferometer and classical chopper tests alternating between hot and cold sources. As shown in Fig. 5(a) this instrument, called sky simulator, comprises a large black disk having the same dimensions as the telescope focal plane. This disk is cooled and simulates the background temperature in ground based observing conditions. The cooling of the background disk is achieved by using a single stage pulse-tube refrigerator enabling a background temperature of 50 K. Additionally, to simulate an astronomical source, a high emissivity ball is placed in front of the black disk and mounted on a motorized XY stage enabling movement with respect to the fixed disk, see Fig. 5(b). The sky simulator disk temperature can be adjusted continuously between 50 K and 300 K allowing an accurate estimation of the detector response and a direct estimation of the Noise Equivalent Temperature (NET).

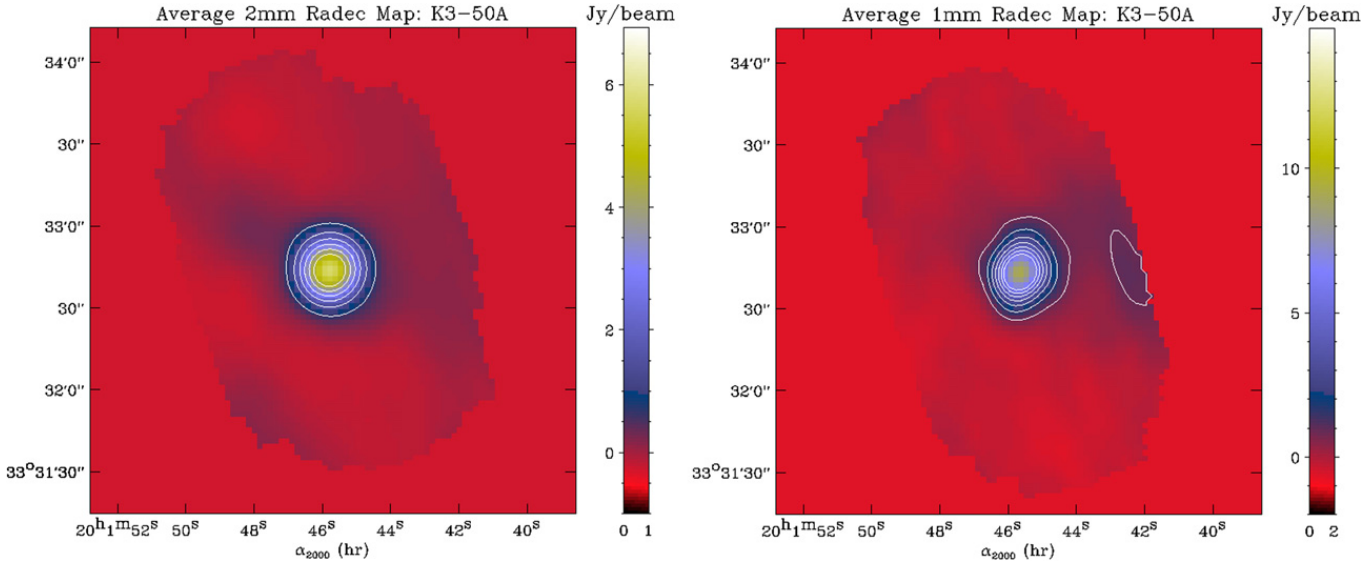

Fig. 6. Maps of K3-50A, an ultra-compact HII region at 2 and 1.4 mm. The measured fluxes are 6.6 ± 0.2 Jy and 14.0 ± 0.3 Jy.

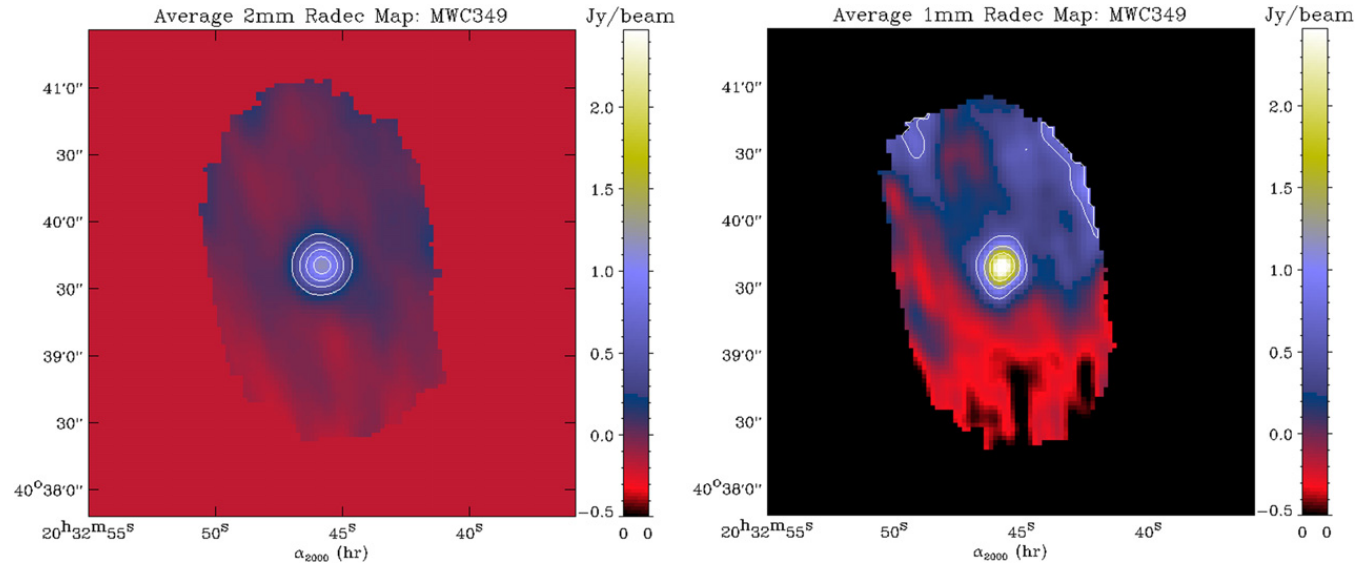

Fig. 7. Maps of MWC 349 at 2 and 1.4 mm. The source is a peculiar star with a bright radio continuum [18]. The measured fluxes are 1.1 ± 0.1 Jy and 3.1 ± 0.3 Jy.

5. Recent astronomical results

The last NIKA run took place in October 2010. The instrument was installed into the receiver cabin of the IRAM 30 meter telescope at Pico Veleta and operated remotely from the control room. The cool-down was also performed remotely, taking approximately 18 hours to reach the operating temperature of 70 mK.

Data from the two arrays are reduced off-line with a dedicated IDL set of routines. For each detector, the raw data (I, Q) are internally converted to the instantaneous resonance frequency which is assumed to be linear with the absorbed photon counts. After opacity correction, we use scans of Mars as a primary calibrator. The Mars scans also give the focal plane geometry and allow us to derive a FWHM angular resolution of 16 and 12.5 arcseconds for the two arrays at 2 and 1.4 mm, respectively. This resolution is the diffraction limit set by the telescope. At this stage, the photometry is not better than 30% due to some instabilities in the detector set up (calibration procedures have not stabilized yet owing to the new type of detectors being used). Noise Equivalent Flux Density (NEFD) is derived by combining known flux sources (e.g. planets) calibration and the RMS noise on blank fields maps.

Figs. 6 and 7 show the two maps at 2 and 1.4 mm for two bright point sources K3-50A and MWC 349. These were obtained by coadding the individual maps of each detector. They show that the pointing reconstruction is quite accurate.

Figs. 8 and 9 show the map of two much weaker sources VCLS 147 and IRC +10420. They illustrate the camera capacity to detect faint point sources.

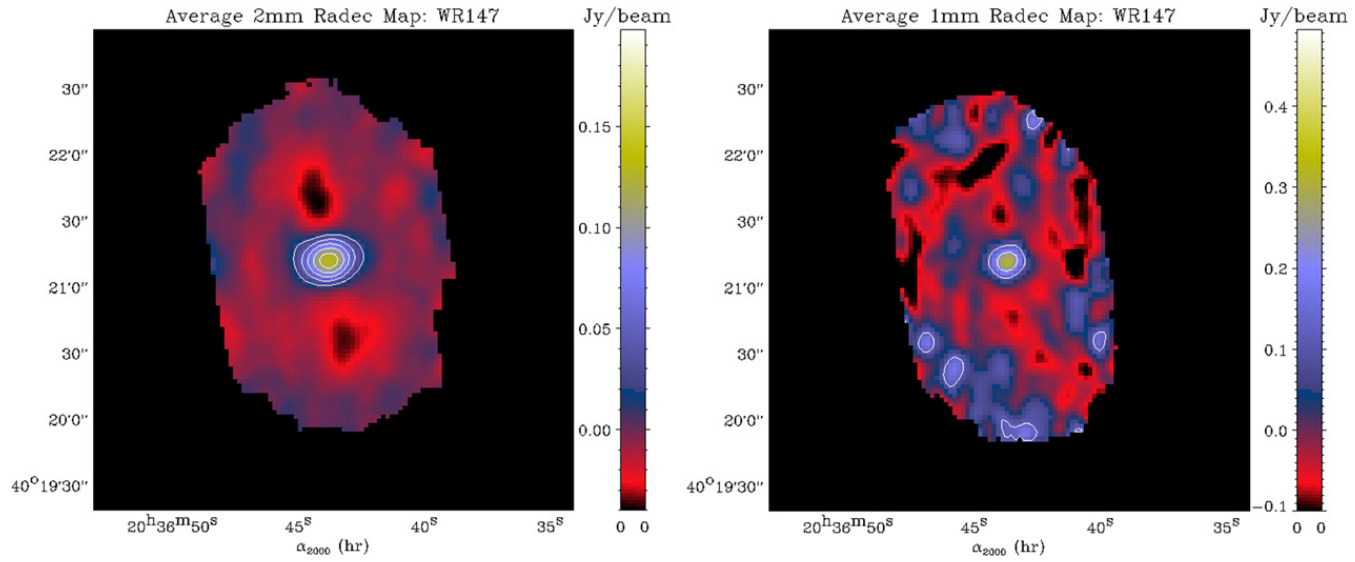

Fig. 8. Maps of VCLS 147, a Wolf–Rayet radio star. The two symmetric negative lobes are an artefact of the filtering procedure. The measured fluxes are 162 ± 12 mJy and 410 ± 66 mJy, the latter being in agreement with Altenhoff et al. [19].

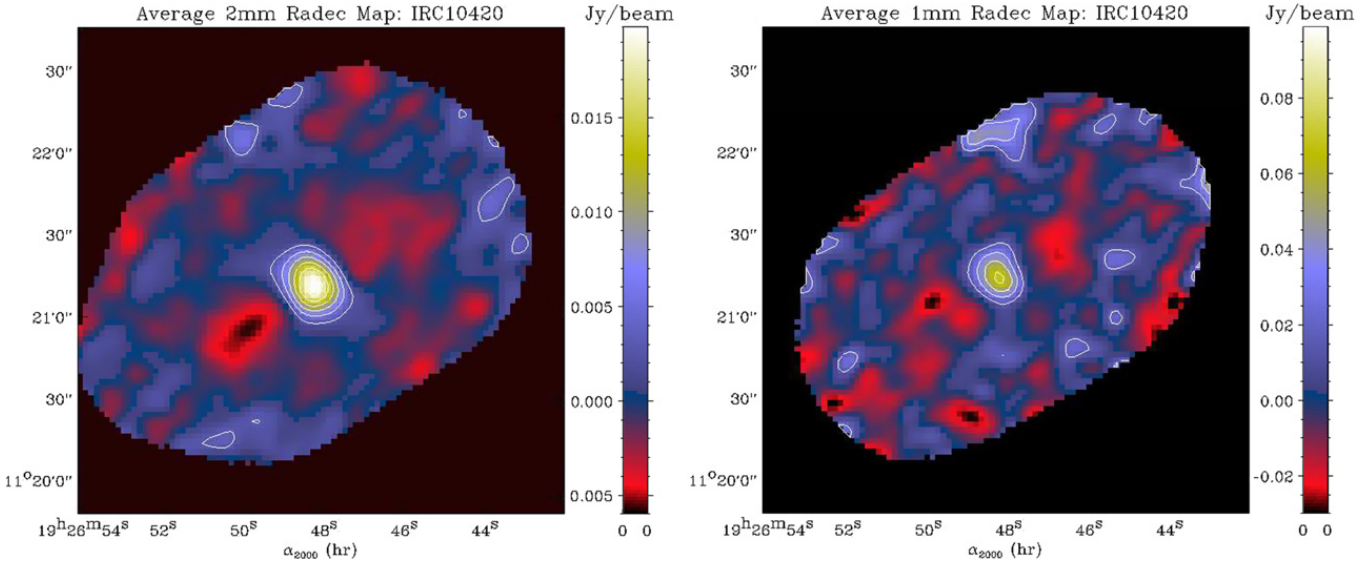

Fig. 9. Maps of IRC +10420, an F-type supergiant star. The measured fluxes are 22.2 ± 1.4 mJy and 104 ± 13 mJy. The maps were obtained with an observation time of half-an-hour. There is a disagreement with the 1.2 mm flux (461 ± 28 mJy) reported by Dehaes et al. [20].

The maps of Cas A, a supernova remnant, are given in Fig. 10. They show the mapping capability of this new camera with a vivid example of extended diffuse emission.

6. Conclusions and plans

We have presented recent developments in the exciting field of kinetic inductance detectors for astronomical applications. For the first time, we have demonstrated with NIKA that KID-based instrument can achieve sensitivities, in real observing conditions, comparable with the more classical bolometers. In particular, the Noise Equivalent Flux Density (NEFD) measured for the 2 mm NIKA channel was, on average, 37 mJy $s^{0.5}$, similar to the MAMBO-2 (semiconducting bolometers, operating at 1.25 mm, 128 pixels) continuum instrument installed permanently at Pico Veleta on the 30 meter telescope. One important advantage of NIKA, compared to MAMBO-2, is represented however by the fact that our focal plane is entirely filled, while MAMBO-2 is horn-coupled, and thus has non-sensitive areas between the different horns. As far as the 1.4 mm NIKA channel is concerned, the sensitivity was not competitive (NEFD = 450 mJy $s^{0.5}$) during the last run. However, we have recently tested in laboratory, using our sky simulator, 1.25 mm optimized arrays exhibiting pixel sensitivities below 40 mJy $s^{0.5}$.

IRAM recently issued a call to build a large field-of-view (6 arcminutes) dual-band resident camera to be installed by the end of 2014. The NIKA consortium is proposing a scaled-up version of the prototype instrument described in this paper. The total number of pixels will be around 4000, with photon-noise limited performances. One crucial point to be addressed

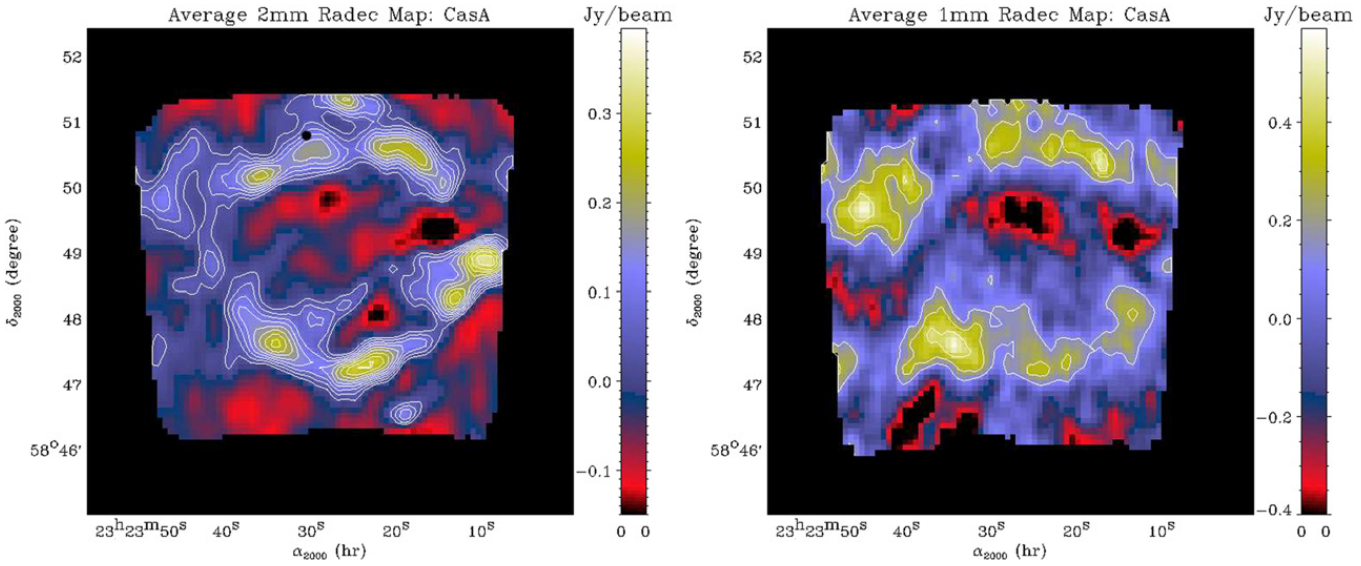

Fig. 10. Maps of Cassiopeia A (Cas A), a young (330 year old) supernova remnant, at 2 and 1.4 mm. The contours at 2 mm are at levels of 32, 63, 95, 127, and 158 mJy/beam. The contours at 1.4 mm are at levels of 142, 285, 427, 569, 712 and 854 mJy/beam. The negative brightness features come from the filtering which is applied in order to reduce the sky noise. The complete analysis of these maps is deferred, in particular the comparison with the dust submillimeter emission as observed by Dunne et al. [21] and the synchrotron radio emission.

is the photometric accuracy; in order to achieve the final goal of less than 5%, we are considering the use of an internal calibrator.

Acknowledgements

We acknowledge the crucial contributions of our collaborators, or ex-collaborators, Loren Swenson, Angelo Cruciani, Christian Hoffmann, Philippe Camus, Karl Schuster, Samuel Leclercq. We also acknowledge the technical staff at Institut Néel that have built the NIKA cryostat and participated in the electronics development, in particular Henri Rodenas, Gregory Garde, Anne Gerardin, Julien Minet and in general the Cryogenics and Electronics Groups. We would like to thank the IRAM-Spain and IRAM-Grenoble staff for the first-class support before, during and after the telescope run. This work was supported in part by grant ANR-09-JCJC-0021-01 of the French National Research Agency (ANR), the Nanosciences Foundation of Grenoble and Région Rhone-Alpes (program CIBLE 2009). Part of the travel funds for the run have been provided by the French Ministère des Affaires étrangères et européennes (PHC Alliance 2010).

References

[1] A.A. Penzias, R.W. Wilson, A measurement of excess antenna temperature at 4080 Mc/s, Astrophysical Journal 142 (1) (1965) 419–421.
[2] P. de Bernardis, P.A.R. Ade, J.J. Bock, J.R. Bond, J. Borrill, A. Boscaleri, K. Coble, B.P. Crill, G. De Gasperis, P.C. Farese, P.G. Ferreira, K. Ganga, M. Giacometti, E. Hivon, V.V. Hristov, A. Iacoangeli, A.H. Jaffe, A.E. Lange, L. Martinis, S. Masi, P.V. Mason, P.D. Mauskopf, A. Melchiorri, L. Miglio, T. Montroy, C.B. Netterfield, E. Pascale, F. Piacentini, D. Pogosyan, S. Prunet, S. Rao, G. Romeo, J.E. Ruhl, F. Scaramuzzi, D. Sforna, N. Vittorio, A flat universe from high-resolution maps of the cosmic microwave background radiation, Nature 404 (6781) (April 2000) 955–959.
[3] M. Birkinshaw, The Sunyaev–Zel'dovich effect, Physics Reports—Review Section of Physics Letters 310 (2–3) (March 1999) 98–195.
[4] A.L. Woodcraft, Scuba-2: a 10,000-pixel submillimetre camera for astronomy, in: 2007 Joint 32nd International Conference on Infrared and Millimeter Waves and 15th International Conference on Terahertz Electronics, vols. 1 and 2, IEEE MTTS, 2007.
[5] G. Siringo, E. Kreysa, A. Kovacs, F. Schuller, A. Weiss, W. Esch, H.P. Gemuend, N. Jethava, G. Lundershausen, A. Colin, R. Guesten, K.M. Menten, A. Beelen, F. Bertoldi, J.W. Beeman, E.E. Haller, The large APEX bolometer camera LABOCA, Astronomy and Astrophysics 497 (3) (April 2009) 945–962.
[6] P.K. Day, H.G. LeDuc, B.A. Mazin, A. Vayonakis, J. Zmuidzinas, A broadband superconducting detector suitable for use in large arrays, Nature 425 (6960) (October 2003) 817–821.
[7] J. Majer, J.M. Chow, J.M. Gambetta, J. Koch, B.R. Johnson, J.A. Schreier, L. Frunzio, D.I. Schuster, A.A. Houck, A. Wallraff, A. Blais, M.H. Devoret, S.M. Girvin, R.J. Schoelkopf, Coupling superconducting qubits via a cavity bus, Nature 449 (7161) (September 2007) 443–447.
[8] P.R. Maloney, N.G. Czakon, P.K. Day, T.P. Downes, R. Duan, J. Gao, J. Glenn, S.R. Golwala, M.I. Hollister, H.G. LeDuc, B.A. Mazin, S.G. McHugh, O. Noroozian, H.T. Nguyen, J. Sayers, J.A. Schlaerth, S. Siegel, J.E. Vaillancourt, A. Vayonakis, P. Wilson, J. Zmuidzinas, Music for sub/millimeter astrophysics, in: Millimeter, Submillimeter, and Far-Infrared Detectors and Instrumentation for Astronomy V, in: Proc. SPIE, vol. 7741, 2010.
[9] A. Monfardini, L.J. Swenson, A. Bideaud, F.X. Désert, S.J.C. Yates, A. Benoit, A.M. Baryshev, J.J.A. Baselmans, S. Doyle, B. Klein, M. Roesch, C. Tucker, P. Ade, M. Calvo, P. Camus, C. Giordano, R. Guesten, C. Hoffmann, S. Leclercq, P. Mauskopf, K.F. Schuster, NIKA: A millimeter-wave kinetic inductance camera, Astronomy and Astrophysics 521 (2010) A29.
[10] A. Monfardini, A. Benoit, A. Bideaud, L. Swenson, A. Cruciani, P. Camus, C. Hoffmann, F.X. Désert, S. Doyle, P. Ade, P. Mauskopf, C. Tucker, M. Roesch, S. Leclercq, K.F. Schuster, A. Endo, A. Baryshev, J.J.A. Baselmans, L. Ferrari, S.J.C. Yates, O. Bourrion, J. Macias-Perez, C. Vescovi, M. Calvo, C. Giordano, A dual-band millimeter-wave kinetic inductance camera for the IRAM 30 m telescope, Astrophysical Journal Supplement Series 194 (2) (June 2011) 24.
[11] H.G. Leduc, B. Bumble, P.K. Day, B.H. Eom, J.S. Gao, S. Golwala, B.A. Mazin, S. McHugh, A. Merrill, D.C. Moore, O. Noroozian, A.D. Turner, J. Zmuidzinas, Titanium nitride films for ultrasensitive microresonator detectors, Applied Physics Letters 97 (10) (September 2010) 102509.
[12] J. Gao, M. Daal, J.M. Martinis, A. Vayonakis, J. Zmuidzinas, B. Sadoulet, B.A. Mazin, P.K. Day, H.G. Leduc, A semiempirical model for two-level system noise in superconducting microresonators, Applied Physics Letters 92 (21) (May 2008) 212504.

[13] S. Doyle, P. Mauskopf, J. Naylon, A. Porch, C. Duncombe, Lumped element kinetic inductance detectors, Journal of Low Temperature Physics 151 (1–2) (April 2008) 530–536.
[14] M. Roesch, Development of lumped element kinetic inductance detectors for NIKA, in: ISSTT 2011, 2011.
[15] S.J.C. Yates, A.M. Baryshev, J.J.A. Baselmans, B. Klein, R. Guesten, Fast Fourier transform spectrometer readout for large arrays of microwave kinetic inductance detectors, Applied Physics Letters 95 (4) (July 2009) 042504.
[16] L.J. Swenson, J. Minet, G.J. Grabovskij, O. Buisson, F. Lecocq, C. Hoffmann, P. Camus, J.C. Villegier, S. Doyle, P. Mauskopf, M. Roesch, M. Calvo, C. Giordano, S.J.C. Yates, A.M. Baryshev, J.J.A. Baselmans, A. Benoit, A. Monfardini, A fast, ultra-sensitive and scalable detection platform based on superconducting resonators for fundamental condensed-matter and astronomical measurements, in: Low Temperature Detectors, AIP Conference Proceedings 1185 (2009) 84–87.
[17] O. Bourrion, A. Bideaud, A. Benoit, A. Cruciani, J.F. Macias-Perez, A. Monfardini, M. Roesch, L. Swenson, C. Vescovi, Electronics and data acquisition demonstrator for a kinetic inductance camera, Journal of Instrumentation 6 (2011) 6012.
[18] D. Tafoya, Y. Gomez, L.F. Rodriguez, Imaging MWC 349 from 7 millimeters to 90 centimeters, Astrophysical Journal 610 (2) (August 2004) 827–834.
[19] W.J. Altenhoff, C. Thum, H.J. Wendker, Radio-emission from stars – a survey at 250-GHz, Astronomy and Astrophysics 281 (1) (January 1994) 161–183.
[20] S. Dehaes, M.A.T. Groenewegen, L. Decin, S. Hony, G. Raskin, J.A.D.L. Blommaert, Continuum emission around AGB stars at 1.2 mm, Monthly Notices of the Royal Astronomical Society 377 (2) (May 2007) 931–944.
[21] L. Dunne, S. Eales, R. Ivison, H. Morgan, M. Edmunds, Type II supernovae as a significant source of interstellar dust, Nature 424 (6946) (July 2003) 285–287.